THE JOURNAL OF PHYSICAL CHEMISTRY C

Article

pubs.acs.org/JPCC

Theoretical Studies of High-Pressure Phases, Electronic Structure, and Vibrational Properties of $NaNH_2$

Yan Zhong,[†] Huai-Ying Zhou,[†,‡] Chao-Hao Hu,*[,‡,§] Dian-Hui Wang,[‡] and Artem R. Oganov[∥,⊥]

[†]School of Materials Science and Engineering, Central South University, Changsha 410083, P. R. China

[‡]School of Materials Science and Engineering, Guilin University of Electronic Technology, Guilin 541004, P. R. China

[§]International Center for Materials Physics, Chinese Academy of Sciences, Shenyang 110016, P. R. China

[∥]Department of Geosciences and Department of Physics and Astronomy, Stony Brook University, Stony Brook, New York 11794-2100, United States

[⊥]Department of Geology, Moscow State University, 119992 Moscow, Russia

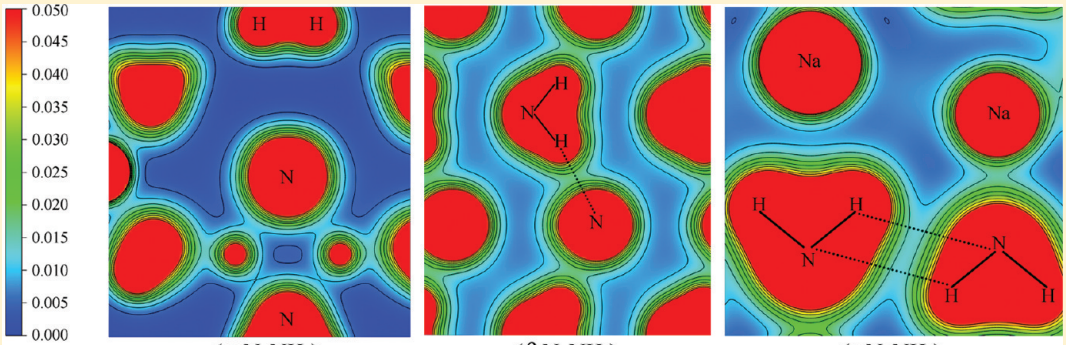

ABSTRACT: Thermodynamically stable phases of sodium amide ($NaNH_2$) at pressures up to 20 GPa have been determined using the ab initio evolutionary structure prediction. We find that the ground-state phase α-$NaNH_2$ (orthorhombic, *Fddd*) first transforms into β-$NaNH_2$ (orthorhombic, $P2_12_12$) at 2.2 GPa; then, γ-$NaNH_2$ (monoclinic, $C2/c$) becomes stable at 9.4 GPa. In addition to strong ionic bonding between Na^+ and $[NH_2]^-$ ions and covalent bonding between H and N in NH_2 groups, the N−H···N hydrogen bonding between neighboring NH_2 groups could not be ignored anymore in the high-pressure β-$NaNH_2$, as suggested by the analysis of charge density distribution and structural and vibrational properties. The covalent N−H bonds in the high-pressure phase of $NaNH_2$ are weakened by additional hydrogen bonding, which could be favorable for the hydrogen desorption.

1. INTRODUCTION

Considerable effort has been devoted to developing feasible and safe hydrogen storage materials that can not only store hydrogen reversibly with high gravimetric and volumetric densities but also allow hydrogen adsorption and desorption under near-ambient conditions.[1−3] Currently, complex metal hydrides, such as borohydrides $M(BH_4)_n$, alanates $M(AlH_4)_n$, and amides $M(NH_2)_n$, have attracted great attention as promising materials for hydrogen storage due to their innately high hydrogen content (for example, 8.7 wt % in $LiNH_2$ and 7.5 wt % in $NaAlH_4$).[4−7] However, these hydrides exhibit such strong metal−hydrogen bonding (B−H, Al−H, and N−H) in the anion subunits (i.e., BH_4^-, AlH_4^-, and NH_2^-) and are so stable that they can be dehydrogenated only at elevated temperatures. Thus, improving the poor dehydrogenation kinetics of the light complex metal hydrides is a critical problem in this field. Experimental studies have verified that the addition of proper catalysts such as TiO_2, Ti_3Al, $TiAl_3$, and $AlCl_3$ is an effective way to reduce the dehydriding temperature of these hydrides. The underlying mechanism of catalysts, however, is not yet fully understood, which prevents further systematic improvements.[8,9] Recently, many high-pressure investigations have been motivated by a theoretical study of Vajeeston et al.,[10] in which a new high-pressure modification of $LiAlH_4$ was found to have accelerated dehydrogenation kinetics accompanied by some structural changes in Al−H bonding. Thus, a detailed study on the high-pressure behavior of these materials is highly desirable.

In recent years, sodium amide ($NaNH_2$) has also attracted considerable attention, although its theoretical hydrogen capacity is only ∼5.1 wt %[11] and obviously lower than that of its counterpart $LiNH_2$. Recent studies have indicated that $NaNH_2$ plays an important role in dehydrogenation of other light metal hydride systems by forming some composite hydrogen storage materials (i.e., $NaNH_2$−$LiAlH_4$,[12] $NaNH_2$−MgH_2,[13] and $NaNH_2$−$LiBH_4$[14]). Structural properties of the

Received: January 14, 2012
Revised: March 3, 2012
Published: April 2, 2012

   dx.doi.org/10.1021/jp300455j | *J. Phys. Chem. C* 2012, 116, 8387−8393

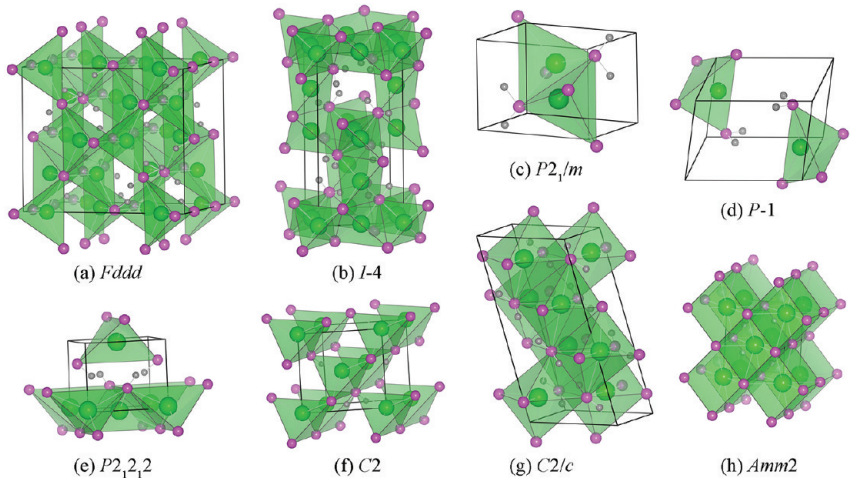

Figure 1. Crystal structures of competing $NaNH_2$ phases: (a) orthorhombic *Fddd* α-$NaNH_2$, (b) tetragonal *I*-4 $LiNH_2$-type, (c) monoclinic $P2_1/m$ KNH_2-type, (d) triclinic *P*-1, (e) orthorhombic $P2_12_12$, (f) monoclinic *C*2, (g) monoclinic *C*2/*c*, and (h) orthorhombic *Amm*2. The large, medium, and small spheres are Na, N, and H, respectively.

ambient-pressure phase of $NaNH_2$ (hereafter, α-$NaNH_2$) have been extensively studied by X-ray and neutron diffraction experiments.[15,16] Under ambient conditions, α-$NaNH_2$ crystallizes in an orthorhombic lattice (space group *Fddd*) with lattice parameters: a = 8.949 Å, b = 10.456 Å, and c = 8.061 Å.[16] The Na atoms are located at the 16f positions, N at the 16g positions, and H at the 32f sites, and the structure contains NaN_4 tetrahedra with Na−N distances of 2.4 to 2.5 Å. The electronic structure of α-$NaNH_2$ has been studied by Tsumuraya et al.[17] using ab initio methods. However, there have been very few studies of the high-pressure behavior of this compound. Recently, Liu et al.[18] have found pressure-induced phase transformations of $NaNH_2$ based on high-pressure Raman and infrared (IR) spectroscopies. Under compression, two phase transitions occur at about 0.9 and 2.0 GPa, as evidenced by the changes in the characteristic Raman and IR modes. However, detailed structural characterization of the high-pressure polymorphs is extremely lacking. In addition, an open issue is whether pressure leads to the formation of hydrogen bonds between the neighboring NH_2 groups in alkali metal amides. Hydrogen bond is considered to play a significant role in altering their physical and chemical properties including frequency shifts of IR and Raman bands.[19] In our previous study on $LiNH_2$,[20] hydrogen bonding was confirmed in high-pressure phase. The existence of hydrogen bond is expected to weaken the N−H polar covalent bonds in amides ions.

In this work, we identify the energetically favorable high-pressure structures of $NaNH_2$ up to 20 GPa using ab initio evolutionary structure searches and further conduct a systematic theoretical study of pressure-induced structural transitions, electronic structure, and lattice vibrational properties by first-principles total-energy calculations.

2. COMPUTATIONAL DETAILS

To find the most stable structures at different pressures, we employed an ab initio evolutionary algorithm (EA), as implemented in the USPEX (Universal Structure Predictor: Evolutionary Xtallography) code.[21,22] This method has been widely used to predict stable high-pressure crystal structures without requiring any experimental information.[23−25] In the present work, variable-cell structure simulations for $NaNH_2$ with one to four formula units (f.u.) were performed at 0, 10, and 20 GPa without any symmetry constraints. The first generation of structures was randomly produced. Each subsequent generation was obtained from the lowest-enthalpy 60% structures of the preceding generation by applying variation operators including heredity (65% structures), lattice mutation (25%), and atomic permutation (10%).

The underlying total-energy calculations were carried out with the Vienna ab initio simulation package (VASP), in the framework of density functional theory (DFT)[26] using a plane-wave basis set.[27,28] The exchange-correlation term was approximated by the Perdew−Burke−Ernzerhof (PBE)[29] functional, and the all-electron projected augmented wave (PAW) approach[30] was used to describe the core electrons and their effect on valence orbitals. The valence states used were $2p^63s^1$ for Na, $2s^22p^3$ for N, and $1s^1$ for H. Plane-wave kinetic energy cutoff of 600 eV and the *k*-point meshes with resolution better than 2π*0.03 $Å^{-1}$ in the reciprocal space were used. Structural optimizations for cell geometry and atomic positions were performed until the self-consistent total energy is converged to 10^{-5} eV/cell, and the force on each atom is $<10^{-3}$ eV/Å.

The phonon calculations were performed using the frozen phonon method as implemented in the FROPHO code.[31] In this method, the atoms in the crystal are displaced with respect to their equilibrium positions, subject to constraints imposed by crystal symmetry, and the resulting Hellmann−Feyman forces are obtained through DFT calculations.[32,33] The force constant matrices were calculated in the 1 × 1 × 2, 2 × 2 × 2, and 2 × 2 × 2 supercells for α-, β-, and γ-$NaNH_2$, respectively, using the Parlinski−Li−Kawazoe method[34] with a finite atomic displacement of ±0.01 Å.

3. RESULTS AND DISCUSSION

In the pressure range of 0−20 GPa, seven energetically competing structures are detected in our evolutionary structure searches for $NaNH_2$ with different unit cells. They are, namely, the ground-state orthorhombic *Fddd* α-$NaNH_2$, monoclinic $P2_1/m$ (KNH_2-type structure), triclinic *P*-1, orthorhombic $P2_12_12$, monoclinic *C*2, monoclinic *C*2/*c*, and orthorhombic *Amm*2 structures. Considering the structural similarity among alkali metal amides, the tetragonal *I*-4 $LiNH_2$-type structure is also explored. As shown in Figure 1, except for the *C*2/*c* and

dx.doi.org/10.1021/jp300455j | J. Phys. Chem. C 2012, 116, 8387−8393

*Amm*2 phases, all proposed structures are composed of slightly distorted NaN_4 tetrahedra in various packing arrangements and NH_2 amide group in different orientations. In the structurally distinct *C*2/*c* and *Amm*2 phases, the distorted Na-centered NaN_6 octahedra and NaN_8 cubes, respectively, are the building blocks. One has to remark the orientational disorder of NH_2 groups in the ambient-pressure α-$NaNH_2$ and pressure-induced ordering appearing in its high-pressure competing phases like the $P2_12_12$, *C*2/*c*, and *Amm*2 structures. For instance, the layered $P2_12_12$ structure is composed of a layer of Na^+ ions sandwiched between two NH_2 layers. The *C*2/*c* structure also has a layered packing of Na^+ ions and NH_2^- groups but is less ordered than the $P2_12_12$ and *Amm*2 structures.

The structural stability is investigated by calculating the free energy of competing phases. In present work, all total-energy calculations are performed at zero temperature. Therefore, the Gibbs free energy becomes equal to the enthalpy, $H = E_0 + PV$, where E_0 is the internal energy of the system. The calculated enthalpy difference (ΔH) relative to α-$NaNH_2$ as a function of pressure is displayed in Figure 2. As observed in the recent

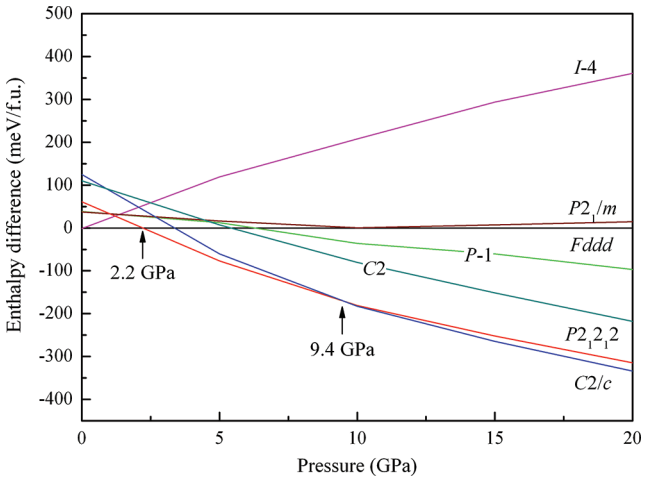

Figure 2. Calculated enthalpies relative to α-$NaNH_2$ as a function of pressure for various structures. The structural transition points induced by pressure are marked by arrows.

high-pressure experiment,[18] two pressure-induced transitions in $NaNH_2$ occur upon pressure increase. The first transformation from α-$NaNH_2$ to $P2_12_12$ phase (hereafter, β-$NaNH_2$) occurs at 2.2 GPa. Above 9.4 GPa, the *C*2/*c* phase (hereafter, γ-$NaNH_2$) becomes more stable than β-$NaNH_2$. The *Fddd*→$P2_12_12$→*C*2/*c* (α→β→γ) structural transition sequence clearly indicates a decrease in symmetry of $NaNH_2$ with pressure. This result is very similar to our previous prediction for the high-pressure behavior of a related compound $LiNH_2$ (*I*-4→*Fddd*→$P2_12_12$)[20] and also agrees with the proposal by Chellappa et al. from the high-pressure Raman spectroscopy experiments on $LiNH_2$,[35] although the predicted transition pressures (around 2.2 GPa for α→β and 9.4 GPa for β→γ) are several GPa higher than the experimental observations (0.9 and 2.0 GPa).

Figure 3 shows the pressure−volume relation of $NaNH_2$ derived by fitting the third-order Birth−Murnaghan equation of state.[36] The α→β transition for $NaNH_2$ is accompanied by a large volume shrinkage of ∼11.3%, which is much larger than the volume contraction (4.5%) induced by the same transition for $LiNH_2$.[20] The occurrence of structural transition from orientationally disordered α phase to ordered β phase needs

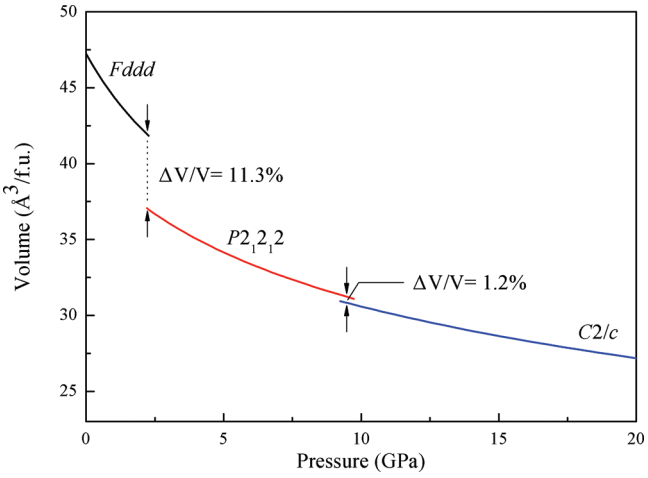

Figure 3. Calculated volume−pressure relationship for $NaNH_2$ polymorphs.

substantial structural modifications in α phase (i.e., breaking and reforming Na−N bonds). This means that the α→β transition is sluggish and reconstructive. The β→γ transition with volume reduction of 1.3% is expected to be a displacive phase transition, which can be easily realized by slightly adjusting the atomic position of Na ions and orientation of NH_2 amide groups.

The optimized equilibrium lattice constants and internal atomic positions for α- (0 GPa), β- (2.2 GPa), and γ-$NaNH_2$ (9.4 GPa) are listed in Table 1. Theoretical structural parameters for α-$NaNH_2$ are in good agreement with the experimental values. The characteristic geometries of amide ions in β- (2.2 GPa), and γ-$NaNH_2$ (9.4 GPa) are shown in Figure 4. The neighboring NH_2 groups in β-$NaNH_2$ are perpendicular to each other, and each N−H bond is aligned almost linearly with the N atom on its neighboring NH_2 group, forming the N−H···N bond. The calculated N−H···N bond angle is ∼164.8° at 2.2 GPa (Figure 4a). For γ-$NaNH_2$ displayed in Figure 4b, two neighboring NH_2 groups approximately lie on a plane, and the four N−H bonds form a parallelogram with the N−H···N bond angle of 117.2° at 9.4 GPa. The intermolecular N···H distances in β- (2.2 GPa) and γ-$NaNH_2$ (9.4 GPa) are 2.472 and 2.413 Å, respectively, which is significantly less than the sum of the van der Waals radii of N and H (2.75 Å).[37] As a result, the formation of hydrogen bond in $NaNH_2$ under compression is possible due to the specific orientation of amide anions and short intermolecular N···H distances, which can also be understood from our latter analysis on electronic structure and vibrational properties of $NaNH_2$. In addition, as suggested in Figure 4, the strength of the approximately linear N−H···N bond in β-$NaNH_2$ is expected to be stronger than that of the bent N−H···N bond in γ-$NaNH_2$.

Figure 5 shows the changes in the nearest intermolecular N···H distance ($d_{N\cdots H}$), intramolecular N−H bond length (d_{N-H}), and H−N−H bond angle ($\angle_{H-N-H}$) with the applied pressure for α-, β-, and γ-$NaNH_2$. The $d_{N\cdots H}$ as a function of pressure in α-$NaNH_2$ is not shown in Figure 5 because there are no direct atomic contacts between N and H on the neighboring NH_2 groups in this phase. The intramolecular N−H bond length d_{N-H} in α-$NaNH_2$ is highly compressed and reduced from 1.031 Å at 0 GPa to 1.016 Å at 20 GPa, whereas in the high-pressure phases, the corresponding reduction is only

dx.doi.org/10.1021/jp300455j | J. Phys. Chem. C 2012, 116, 8387−8393

Table 1. Optimized Structural Parameters of α- (0 GPa), β- (2.2 GPa), and γ-$NaNH_2$ (9.4 GPa)[a]

			atomic coordinates (fractional)		
structure	lattice parameters (Å, deg)		x	y	z
α-$NaNH_2$ ($Fddd$)	a = 8.907 (8.949)	Na:	0.0000	0.1407 (0.1452)	0.0000
Z = 16	b = 10.726 (10.456)	N:	0.0000	0.0000	0.2328 (0.2365)
	c = 8.289 (8.061)	H:	0.0442 (0.0635)	0.9352 (0.9034)	0.3113 (0.3053)
β-$NaNH_2$ ($P2_12_12$)	a = 4.307	Na:	0.0000	0.0000	0.5021
Z = 2	b = 4.328	N:	0.0000	0.5000	0.7898
	c = 3.973	H:	0.1311	0.6305	0.9549
γ-$NaNH_2$ ($C2/c$)	a = 5.022	Na:	0.0000	0.3285	0.7500
Z = 4	b = 5.246	N:	0.0000	0.2222	0.2500
	c = 4.839	H:	0.1158	0.0993	0.3972
	β = 104.867				

[a]For comparison, the experimental values for α-$NaNH_2$ from ref 16 are given in parentheses.

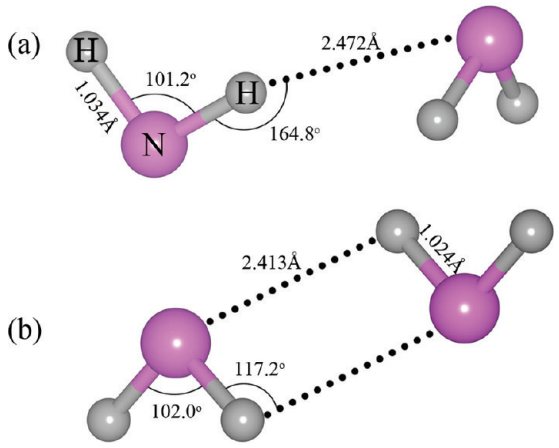

Figure 4. Geometries of amide ions in (a) β-$NaNH_2$ at 2.2 GPa and (b) γ-$NaNH_2$ at 9.4 GPa.

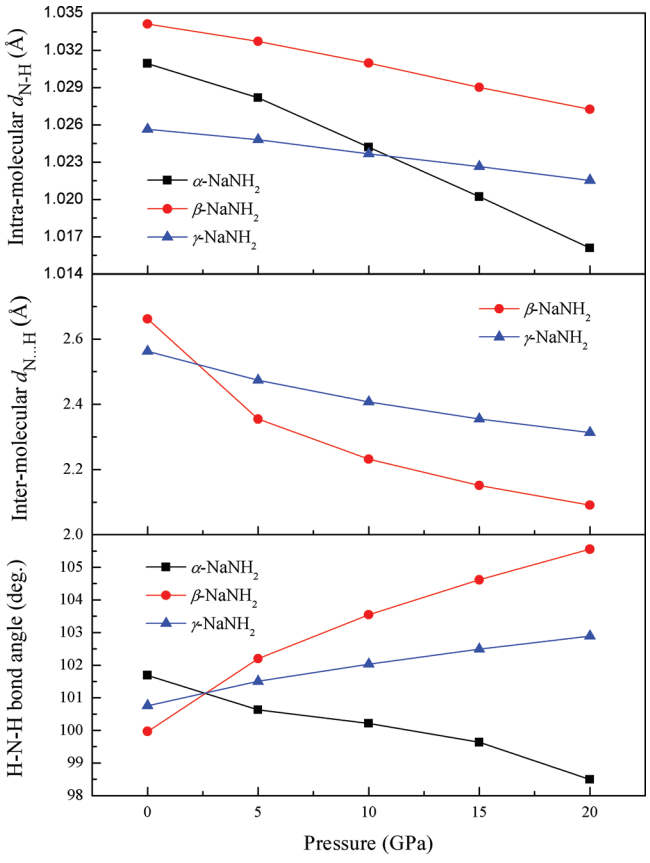

Figure 5. Changes of intramolecular N−H distance (d_{N-H}) in NH_2 groups, intermolecular N···H length ($d_{N\cdots H}$) between neighboring NH_2 groups, and H−N−H bond angle with pressure in $NaNH_2$.

about 0.007 and 0.004 Å, which may be partially attributed to the resistance against pressure effect resulting from the hydrogen bonding in these two phases. Notably, in β-$NaNH_2$, d_{N-H} is larger than in α- and γ-$NaNH_2$ in the whole pressure range considered here. This means that the strength of N−H bond in each NH_2 group in β-$NaNH_2$ is lower than that in α and γ phases. The weakening of N−H bond may facilitate the hydrogen release from β-$NaNH_2$. We also note that in the high-pressure phases, especially in β-$NaNH_2$, the $\angle_{H-N-H}$ angle increases during compression; a similar phenomenon has been observed in hydrogen-bonded systems like water in bikitaite.[38] Data presented in Figure 5 imply that β-$NaNH_2$ has rather strong N−H···N hydrogen bonds.

To further analyze the nature of chemical bonding in $NaNH_2$, we present the total density of states (DOS) and partial DOS of α, β, and γ phases at different pressures in Figure 6. All three phases are insulators with a finite energy band gap (E_g) between the valence band (VB) and conduction band (CB). The calculated DFT band gap E_g for α- (at 0 GPa), β- (at 2.2 GPa), and γ-$NaNH_2$ (at 9.4 GPa) are 2.0, 2.9, and 3.1 eV, respectively. Note that it is well known that DFT underestimates band gaps. The VBs are mostly composed of N 2p and H 1s states, while the contribution from Na is negligible. Therefore, even upon compression $NaNH_2$ is predominantly an ionic solid with the ionic interaction between Na^+ cations and the $[NH_2]^-$ anion complexes. The N 2p and H 1s states are energetically degenerate in the VB region, which indicates that the N−H hybridization is remarkable and there is strong covalent bonding between N and H in the $[NH_2]^-$ subunits. It can also be found from Figure 6 that there is no obvious difference in DOS between the α- and β-$NaNH_2$. Their VBs are split into three separate regions in the range from −8 to 0 eV, except for a little difference in peak profiles. On going from β- to γ-$NaNH_2$ the DOS peaks in the VB region become broader, which mainly originates from the increase of the density and modification of the coordination environment in $NaNH_2$ (i.e., NaN_4 tetrahedra in β vs NaN_6 octahedra in γ). This broadening shows that electronic delocalization in γ-$NaNH_2$ increases under the influence of pressure. Moreover, the E_g gradually increases accompanying the $\alpha \rightarrow \beta \rightarrow \gamma$

dx.doi.org/10.1021/jp300455j | J. Phys. Chem. C 2012, 116, 8387−8393

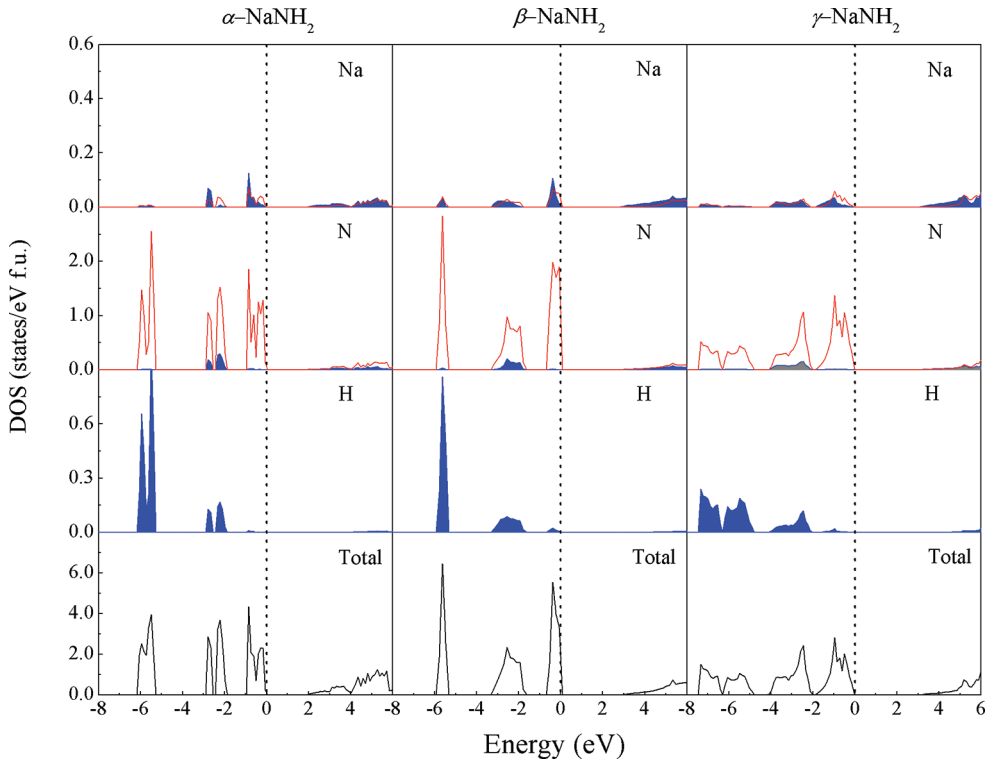

Figure 6. Calculated total and partial density of states for α- (at 0 GPa), β- (at 2.2 GPa), and γ-$LiNH_2$ (at 9.4 GPa). Fermi levels are set to zero energy and marked by dotted vertical lines; s and p states are shaded-blue areas and red lines, respectively.

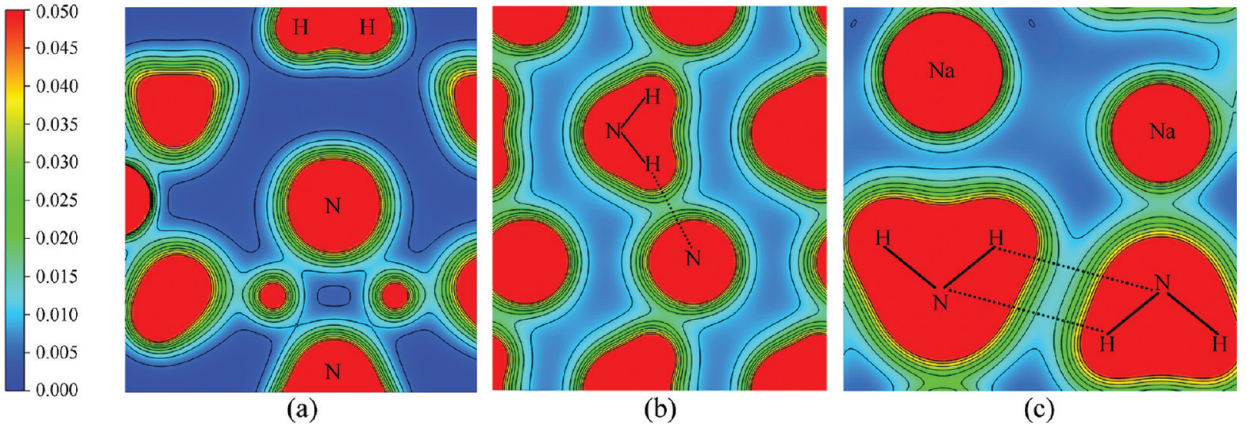

Figure 7. Charge density distribution of $NaNH_2$ within the scale of 0 to 0.05 $e/Å^3$: (a) the slice across the NH_2 group for α-$NaNH_2$ at 0 GPa, (b) the slice across the NH_2 group and its neighboring N atoms for β-$NaNH_2$ at 2.2 GPa, and (c) the slice across the neighboring NH_2 groups for γ-$NaNH_2$ at 9.4 GPa. The hydrogen bond paths are denoted by the dotted lines.

transitions, which suggests that the ionic interaction in $NaNH_2$ will become even more prominent upon compression.

To probe the existence of hydrogen bonding in $NaNH_2$, we calculated the charge density distribution (CDD). The calculated CDDs for some selected planes across the NH_2 groups for α- (at 0 GPa), β- (at 2.2 GPa), and γ-$NaNH_2$ (at 9.4 GPa) are displayed in Figure 7a–c. The CDDs show that the bonding interaction between Na and NH_2 group is ionic, and a strong polarized covalent bond exists between N and H atoms in NH_2 groups. In addition, the possibility of the existence of hydrogen bonding in $NaNH_2$ can be confirmed by investigating the charge density (ρ) at the bond critical point (bcp). As pointed out by Scheiner,[39] hydrogen bond exists as long as the electron density ρ_{bcp} at the bcp is in the range of 0.01 to 0.03 $eÅ^{-3}$. As shown in Figure 7b,c, the ρ_{bcp} in β- and γ-$NaNH_2$ are observable and about 0.019 and 0.015 $eÅ^{-3}$, respectively, which meets the criterion of the formation of hydrogen bond. In contrast with this, the ρ_{bcp} in α-$NaNH_2$ (see Figure 7a) is 0.002 $eÅ^{-3}$, indicating no hydrogen bonding in this phase.

The calculated phonon density of states (PDOS) for α-, β-, and γ-$NaNH_2$ at different pressures is presented in Figure 8. The absence of imaginary frequencies in all PDOSs reveals that the three phases are dynamically stable. Similar to the experimental Raman spectra of $NaNH_2$[18] and other amides such as $LiNH_2$[35] and KNH_2,[40] the calculated PDOSs for $NaNH_2$ are mainly grouped into three frequency bands, which correspond to the complex translational and librational motions of Na^+ cations and $[NH_2]^-$ anions, the bending mode (ν_2) induced by H–N–H bond angle, and the N–H symmetric (ν_1) and asymmetric stretching modes (ν_3), respectively. The

dx.doi.org/10.1021/jp300455j | J. Phys. Chem. C 2012, 116, 8387–8393

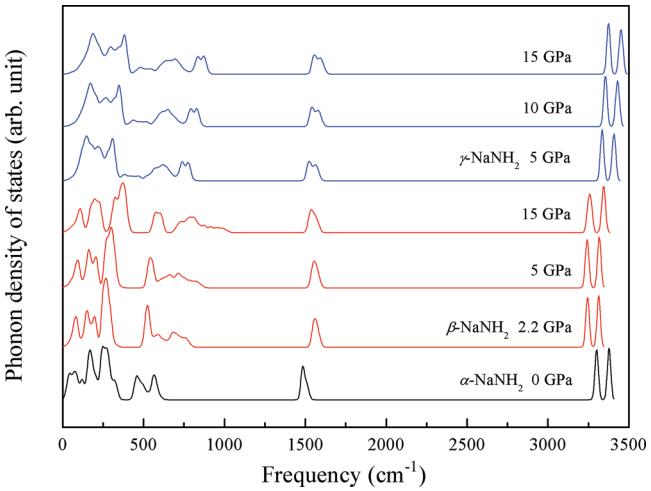

Figure 8. Calculated phonon densities of states (PDOS) for $NaNH_2$ at different pressures. Bottom spectrum is the PDOS of α-$NaNH_2$ at 0 GPa. The middle and top three spectra are the PDOSs of β- and γ-$NaNH_2$, respectively.

calculated peaks of PDOS for α-$NaNH_2$ at 0 GPa are as follows: bending frequency ν_2 = 1482 cm^{-1}, symmetric stretching frequency ν_1 = 3302 cm^{-1}, and asymmetric stretching ν_3 = 3375 cm^{-1}, which are in good agreement with the previous Raman spectra experiments by Cunningham et al.[41] and Liu et al.[18] However, the pressure-induced changes in the PDOSs of the three structures also exhibit significant differences. In the low-frequency region, all lattice modes in β- and γ-$NaNH_2$ significantly broaden and shift to higher frequency with increasing pressure, especially for the librational modes. Previous neutron scattering studies on $NaNH_2$ have suggested that the librational motions at about 400 and 550 cm^{-1} are mainly ascribed to the wagging and torsion of $[NH_2]^-$ ions, and the vibronic coupling can be found at these frequencies.[42] Considerable broadening of these lattice modes is due to the significant modifications of the $[NH_2]^-$ ions and vibronic coupling of N and H in $[NH_2]^-$ ions in β- and γ-$NaNH_2$. In the medium-frequency region, the H−N−H bending modes show an increase in frequency accompanying the $\alpha \rightarrow \beta \rightarrow \gamma$ transitions. However, for the β and γ phases themselves, the change in H−N−H bending modes upon increasing pressure is very small. In fact, the bending modes ν_2 in β-$NaNH_2$ even slightly shift to lower frequency from 1562 cm^{-1} at 2.2 GPa to 1553 cm^{-1} at 5.0 GPa and then to 1537 cm^{-1} at 15 GPa, which is mostly attributed to the influence of hydrogen bond in this phase. In general, phonon frequencies in solids gradually increase with increasing pressure, but for hydrogen-bonded systems (as in β-$NaNH_2$) the opposite effect can be seen. This inverse effect is even more remarkable for the high-frequency N−H stretching modes in β-$NaNH_2$. The N−H symmetric and asymmetric stretching modes in β-$NaNH_2$ at 2.2 GPa distinctly shift to a lower frequency (ν_1 = 3247 cm^{-1} and ν_3 = 3314 cm^{-1}, respectively). Moreover, the N−H stretching modes in β-$NaNH_2$ reach a minimum at ∼10 GPa and then begin to increase again (ν_1 = 3258 cm^{-1} and ν_3 = 3342 cm^{-1} at 15 GPa). γ-$NaNH_2$ does not show such anomalies, and one can conclude that H-bonding diminishes or disappears altogether upon the $\beta \rightarrow \gamma$ transition. In addition, compared with the PDOSs of β-$NaNH_2$, the lattice modes below 480 cm^{-1} are diffuse and the peaks of librations of $[NH_2]^-$ anions become broad and overlapped in γ-$NaNH_2$. This indicates the orientational disorder in the γ phase is increased, being consistent with the recent experimental observation on $NaNH_2$.[18]

4. CONCLUSIONS

We have performed a comprehensive study of the energetic and structural properties of $NaNH_2$ under compression using ab initio total-energy calculations and evolutionary structure prediction. The known α-$NaNH_2$ phase together with other six energetically competing structures under different pressures has been identified in our evolutionary simulations. Static enthalpy calculations have revealed that $NaNH_2$ undergoes two pressure-induced structural transitions with increasing pressure. The ground-state α-$NaNH_2$ first transforms into an orthorhombic β-$NaNH_2$ with space group $P2_12_12$ at 2.2 GPa and then into a monoclinic γ-$NaNH_2$ with space group $C2/c$ at 9.4 GPa, accompanied by volume reductions of 11.3 and 1.2%, respectively. The predicted structural sequence ($Fddd \rightarrow P2_12_12 \rightarrow C2/c$) of $NaNH_2$ is very similar to the high-pressure behavior of the related compound $LiNH_2$ ($I\text{-}4 \rightarrow Fddd \rightarrow P2_12_12$), suggesting that the trend of lowering symmetry induced by high pressure may be common in alkali metal amides. Calculated DOS and charge density clearly show the ionic interaction between Na and NH_2 groups and covalent bonding within the NH_2 groups. A detailed analysis of the structural, electronic, and vibrational properties of $NaNH_2$ has shown that the N−H···N hydrogen bond emerges in β-$NaNH_2$ but diminishes or disappears in γ-$NaNH_2$. The existence of hydrogen bond in the high-pressure β-$NaNH_2$ weakens the covalent N−H bonds within the NH_2 groups and should facilitate hydrogen release from $NaNH_2$.

AUTHOR INFORMATION

Corresponding Author

*E-mail: chaohao.hu@guet.edu.cn.

Notes

The authors declare no competing financial interest.

ACKNOWLEDGMENTS

We gratefully acknowledge financial support from the National Natural Science Foundation of China (grant nos. 50901023, 50971049, 11164005, and 50961004), the Key Program of Guangxi Natural Science Foundation (grant no. 2010GXNSFD013009), the Research Foundation of Guangxi Key Laboratory of Information, and the project-sponsored by SRF for ROCS, SEM. A.R.O. acknowledges funding from DARPA (grant N66001-10-1-4037) and NSF (grant EAR-1114313).

REFERENCES

(1) Chen, P.; Xiong, Z.; Luo, J.; Lin, J.; Tan, K. L. *Nature* **2002**, *420*, 302−304.
(2) Züttel, A.; Wenger, P.; Rentsch, S.; Sudan, P.; Mauron, Ph.; Emmenegger, Ch. *J. Power Sources* **2003**, *118*, 1−7.
(3) Jensen, C. M.; Gross, K. J. *Appl. Phys. A* **2001**, *72*, 213−219.
(4) Bogdanovic, B.; Brand, R. A.; Marjanovic, A.; Schwickardi, M.; Tölle, J. *J. Alloys Compd.* **2000**, *302*, 36−58.
(5) Weidenthaler, C.; Pommerin, A.; Felderhoff, M.; Bogdanovic, B.; Schüth, F. *Phys. Chem. Chem. Phys.* **2003**, *5*, 5149−5153.
(6) Ichikawa, T.; Hanada, N.; Isobe, S.; Leng, H.; Fujii, H. *J. Phys. Chem. B* **2004**, *108*, 7887−7982.
(7) Nakamori, Y.; Orimo, S. *J. Alloys Compd.* **2004**, *370*, 271−275.
(8) Resan, M.; Hampton, M. D.; Lomness, J. K.; Slattery, D. K. *Int. J. Hydrogen Energy* **2005**, *30*, 1417−1421.

(9) Tsumuraya, T.; Shishidou, T.; Oguchi, T. *Phys. Rev. B* **2008**, *77*, 235114.
(10) Vajeeston, P.; Ravindran, P.; Vidya, R.; Fjellvåg, H.; Kjekshus, A. *Phys. Rev. B* **2003**, *68*, 212101.
(11) Ichikawa, T.; Isobe, S. *Z. Kristallogr.* **2008**, *223*, 660−665.
(12) Xiong, Z. T.; Hu, J. J.; Wu, G. T.; Liu, Y. F.; Chen, P. *Catal. Today* **2007**, *120*, 287−291.
(13) Sheppard, D. A.; Paskevicius, M.; Buckley, C. E. *J. Phys. Chem. C* **2011**, *115*, 8407−84413.
(14) Zhang, Y.; Tian, Q. *Int. J. Hydrogen Energy* **2011**, *36*, 9733−9742.
(15) Juza, R.; Weber, H. H.; Opp, K. *Z. Anorg. Allg. Chem.* **1956**, *284*, 73−82.
(16) Nagib, M.; Kistrup, H.; Jacobs, H. *Atomkernenergie* **1975**, *26*, 87−90.
(17) Tsumuraya, T.; Shishidou, T; Oguchi, T. *J. Phys: Condens. Matter* **2009**, *21*, 185501.
(18) Liu, A.; Song, Y. *J. Phys. Chem. B* **2011**, *115*, 7−13.
(19) Pimentel, G. C.; McClellan, A. L. *The Hydrogen Bond*; W. H. Freeman and Company: San Francisco, 1960.
(20) Zhong, Y.; Zhou, H. Y.; Hu, C. H.; Oganov, A. R.; Wang, D. H.; Lyakhov, A. O.; Rao, G. H. *Phys. Rev. B* **2011**, under review.
(21) Oganov, A. R.; Glass, C. W. *J. Chem. Phys.* **2006**, *124*, 244704.
(22) Glass, C. W.; Oganov, A. R.; Hansen, N. *Comput. Phys. Commun.* **2006**, *175*, 713−720.
(23) Oganov, A. R.; Chen, J.; Gatti, C.; Ma, Y. Z.; Ma, Y. M.; Glass, C. W.; Liu, Z. X.; Yu, T.; Kurakevych, O. O.; Solozhenko, V. L. *Nature* **2009**, *457*, 863−867.
(24) Xie, Y.; Oganov, A. R.; Ma, Y. M. *Phys. Rev. Lett.* **2010**, *104*, 177005.
(25) Hu, C. H.; Oganov, A. R.; Wang, Y. M.; Zhou, H. Y.; Lyakhov, A. O.; Hafner, J. *J. Chem. Phys.* **2008**, *129*, 234105.
(26) Kohn, W.; Sham, L. J. *Phys. Rev.* **1965**, *140*, A1133−A1138.
(27) Kresse, G.; Hafner. *J. Phys. Rev. B* **1994**, *49*, 14251−14269.
(28) Kresse, G.; Furthmüller, J. *Comput. Mater. Sci.* **1996**, *6*, 15−50.
(29) Perdew, J. P.; Burke, K.; Ernzerhof, M. *Phys. Rev. Lett.* **1996**, *77*, 3865−3868.
(30) Kresse, G.; Joubert, D. *Phys. Rev. B* **1999**, *59*, 1758−1775.
(31) Togo, A. http://fropho.sourceforge.net/.
(32) van de Walle, A.; Ceder, G. *Rev. Mod. Phys.* **2002**, *74*, 11−45.
(33) Togo, A.; Fumiyasu, O.; Tanaka., I. *Phys. Rev. B* **2008**, *78*, 1134106.
(34) Parlinski, K.; Li, Z. Q.; Kawazoe, Y. *Phys. Rev. Lett.* **1997**, *78*, 4063−4066.
(35) Chellappa, R. S.; Chandra, D.; Somayazulu, M.; Gramsch, S. A.; Hemley, R. J. *J. Phys. Chem. B* **2007**, *111*, 10785−10789.
(36) Birth, F. *Phys. Rev.* **1947**, *71*, 809−824.
(37) Lutz, H. D. *J. Mol. Struct.* **2003**, *646*, 227−236.
(38) Ferro, O.; Quartieri, S.; Vezzalini, G.; Fois, E.; Gamba, A.; Tabacchi, G. *Am. Mineral.* **2002**, *87*, 1415−1425.
(39) Scheiner, S. *Hydrogen Bonding: A Theoretical Perspective*; Oxford University Press: Oxford, U.K., 1997.
(40) Müller, M.; Asmussen, B.; Press, W.; Senker, J.; Jacobs, H.; Büttner, H.; Schober, H. *J. Chem. Phys.* **1998**, *109*, 3559−3567.
(41) Cunningham, P. T.; Maroni, V. A. *J. Chem. Phys.* **1972**, *57*, 1415−1418.
(42) Day, D. H.; Sinclair, R. N. *J. Chem. Phys.* **1971**, *55*, 2807−2811.